Icarus 354 (2021) 114033

Contents lists available at ScienceDirect

Icarus

journal homepage: www.elsevier.com/locate/icarus

Research paper

Infrared spectra and optical constants of astronomical ices: III. Propane, propylene, and propyne

Reggie L. Hudson [a,*], Perry A. Gerakines [a], Yukiko Y. Yarnall [a,b], Ryan T. Coones [a,c]

[a] Astrochemistry Laboratory, NASA Goddard Space Flight Center, Greenbelt, MD 20771, USA
[b] Universities Space Research Association, Greenbelt, MD 20771, USA
[c] School of Pharmacy, University of Reading, Whiteknights, Reading RG6 6AD, UK

ARTICLE INFO

Keywords:
Ices
IR spectroscopy
TNOs
Titan
Organic chemistry
Infrared observations

ABSTRACT

Infrared (IR) spectra of the hydrocarbon ices C_3H_8 (propane), C_3H_6 (propylene, propene), and C_3H_4 (propyne, methylacetylene) are relevant to the study of the low-temperature chemistry and spectroscopy of objects within and beyond the Solar System, but IR band strengths and absorption coefficients are lacking for these compounds. Here we present new IR spectra of crystalline and non-crystalline forms of C_3H_8, C_3H_6, and C_3H_4. Measurements of ice density and refractive index also are reported, two quantities needed to compute IR absorption coefficients, band strengths, optical constants, and, ultimately, abundances of propane, propylene, and propyne in extraterrestrial environments and in laboratory experiments. Suggestions and interpretations are offered regarding the multiple crystalline forms of propane and propylene observed. Applications and extensions are described.

1. Introduction

Several years ago we reported infrared (IR) optical constants of three 2-carbon hydrocarbon ices, acetylene (C_2H_2), ethylene (C_2H_4), and ethane (C_2H_6), presenting data for amorphous and crystalline forms of each compound (Hudson et al., 2014a; Hudson et al., 2014b). We also presented apparent and absolute IR band strengths, as well as apparent and absolute absorption coefficients, for the solid forms of these compounds known to exist under vacuum conditions. The applications of such data are to laboratory work and observational astronomy, both ground-based and space based. Studies of the chemistry of worlds on which solid hydrocarbons exist, such as Pluto, Titan, and trans-Neptunian objects (TNOs), can benefit from our results in the quantification of ice composition (e.g., Brown et al., 2015; Sasaki et al., 2005). Similarly, laboratory studies of the reaction chemistry of small molecules of planetary and interstellar interest find our work relevant for measuring molecular abundances and reaction yields (e.g., Dartois et al., 2017; Fleury et al., 2019; Behmard et al., 2019).

The astrochemical background and justification for our particular choice of hydrocarbons to study is straightforward and does not need extensive comment. Aliphatic hydrocarbon compounds of the type C_3H_x ($x = 1, 2, 3$) are found in a variety of astronomical environments and are suspected in others. Propane (C_3H_8, $H_3C\text{-}CH_2\text{-}CH_3$) is known to be both meteoritic and a component of Titan's atmosphere (Maguire et al., 1981; Sephton et al., 2001; Roe et al., 2003). Propylene (C_3H_6, $H_2C{=}CH\text{-}CH_3$) also is a Titan molecule, and has been detected in the interstellar medium as well (Marcelino et al., 2007; Nixon et al., 2013). Propyne (C_3H_4, $HC{\equiv}C\text{-}CH_3$) is, again, found at Titan and is interstellar (Snyder and Buhl, 1973; Teanby et al., 2009). Given the presence of methane (CH_4) and ethane (C_2H_6) on Pluto's surface (Cruikshank et al., 2015), and the known tendency for solid CH_4 to yield more-complex hydrocarbons upon ion irradiation, these same three C_3H_x molecules are expected on that world and other TNOs (e.g., Strazzulla et al., 1984; Baratta et al., 2003; Bennett et al., 2006; Hudson et al., 2009). Added to these examples of Solar System hydrocarbons are reports of aliphatic organics, or aliphatic functional groups, on Iapetus, Ceres, and comet 67P (Cruikshank et al., 2014; De Sanctis et al., 2017; Raponi et al., 2020). In some cases, C_3H_x molecules already are known to exist in the gas phase, but they also are suspected in the solid phase where they can undergo reactions to produce both simpler and more-complex chemical species.

The laboratory background and justification for our work is somewhat more convoluted. About 20 years ago our group published a study of cometary hydrocarbons, including propane, formed by ionizing radiation (Moore and Hudson, 1998). An IR band strength given there for propane in an H_2O-ice was measured in a reflection mode for our spectrometer's optical path. That propane band-strength value has since

* Corresponding author at: Astrochemistry Laboratory (Code 691), NASA Goddard Space Flight Center, Greenbelt, MD 20771, USA.
E-mail address: reggie.hudson@nasa.gov (R.L. Hudson).

https://doi.org/10.1016/j.icarus.2020.114033
Received 29 May 2020; Received in revised form 28 July 2020; Accepted 3 August 2020
Available online 10 August 2020
0019-1035/Published by Elsevier Inc.

been used in at least three other investigations, each involving transmission spectroscopy for which our value is not necessarily applicable (de Barros et al., 2011; Mejía et al., 2013; Vasconcelos et al., 2017). A paper from yet a different group described the photochemical formation of propane from solid CH_4, but again a direct measure of an IR band strength for solid-propane was not available from which to calculate propane yields (Gerakines et al., 1996). The situation is different for propylene and propyne in the sense that no laboratory on these solids are available at all.

In the present paper we address these issues by continuing our earlier studies, now reporting new laboratory measurements of the IR intensities and optical constants of three 3-carbon solid hydrocarbons, propane (C_3H_8), propylene (C_3H_6, also called propene), and propyne (C_3H_4, also called methyl acetylene). Results for both the amorphous and crystalline forms of each compound are presented, including the first IR intensity information for each solid, the first tabulation of peak positions for the metastable crystalline phases of C_3H_8 and C_3H_6, and reference solid-phase refractive index and density measurements. Our IR spectra and optical constants are presented both graphically and in electronic form to better facilitate their use.

Our choice of the mid-infrared region for this study is based on the large amount of earlier IR work in this spectral region and the ready ability mid-IR spectra offer for distinguishing and characterizing various solid forms of a compound and the transitions between them. Applications of our results to astronomical observational are possible, but we caution that our ices are not strictly analogs of those in any particular astronomical environment. Infrared band positions and intensities may well change on going from one-component to multi-component ices. However, using our results for reference, one can prepare ice mixtures with accurately known compositions either of several hydrocarbons or solid mixtures rich in H_2O-ice or frozen N_2 from which to extract IR intensities and other information. For two earlier works on hydrocarbon-containing samples, see Bohn et al. (1994) for N_2-rich ices and Lang et al. (2013) for hydrocarbon-containing aerosol particles.

2. Laboratory procedures

The laboratory methods and equipment used were largely the same as in our studies of acetylene, ethylene, and ethane (Hudson et al., 2014a; Hudson et al., 2014b), so only a summary is given here with an emphasis on new procedures. Propane, propylene, and propyne were purchased from Sigma Aldrich (now MilliporeSigma) with stated purities of ≥99% and used as received. Following some exploratory work to identify crystallization temperatures, we used an ultrahigh-vacuum (UHV) system (~10^{-10} Torr) to measure densities and reference refractive indices ($\lambda = 670$ nm) for both amorphous and crystalline forms of each compound, each quantity measured in triplicate or more. The phase or form of each sample was checked with an interfaced Thermo iS50 IR spectrometer. An INFICON quartz-crystal microbalance enabled density measurements to be made during the growth of each ice sample, while two-laser interferometry gave data from which each ice's refractive indices at 670 nm were determined (Tempelmeyer and Mills, 1968; Hudson et al., 2017).

Briefly, for IR intensity measurements hydrocarbon ices were made by vapor-phase deposition onto a pre-cooled CsI or KBr substrate ($T_{min} \sim 8$ K). Transmission IR spectra were recorded at the deposition temperature and after various warmings and coolings. Deposition rates were such as to give an increase in ice thickness of a few micrometers per hour, as measured by laser interferometry. The spectrometer's IR beam was directed perpendicular to each ice sample, with spectra recorded from 7800 to 400 cm^{-1} at a resolution of 0.5 cm^{-1} and 200 scans per spectrum. Higher resolutions could have been employed, but IR features were sufficiently broad that higher resolution carried little, if any, advantage. The focus of this paper is almost entirely on the 5000 to 400 cm^{-1} region, with longer and shorter wavenumbers (and wavelengths) to be studied later with somewhat thicker samples. Unlike in some of our previous work, no evidence of crystallization was seen on deposition near 10 K (e.g., Takeda et al., 1990; Hudson et al., 2014a; Hudson et al., 2014b; Mizuno et al., 2016).

Ices of thicknesses ~0.25 to 2 μm were made from C_3H_8, C_3H_6, and C_3H_4, in order to evaluate apparent absorption coefficients (α') of IR peaks and IR band strengths (A') with the same method use in our recent papers using slopes of the appropriate Beer's Law plots (e.g., Hudson et al., 2014a). See also Hollenberg and Dows (1961). Ices typically sat for 20–30 min at the temperatures given here before spectra were recorded. No evidence for sublimation was observed at the temperatures for which spectra are shown.

The most significant change in the present work was an upgrade in the way we calculated optical constants n and k. The method used in our earlier hydrocarbon studies was updated, expanded, and incorporated into a newly developed computer program written in the Python language. Our code has the advantages of permitting wavenumber-dependent optical constants n and k of a substrate to be used, a stronger method for judging convergence, the ability to handle highly asymmetric IR bands that can be found with amorphous solids, and the ability to handle the very sharp features of crystalline ices. As there is no widely used, open-source software for optical-constants calculations, we intend to make ours publicly available in both Python and Windows-executable versions (Gerakines and Hudson, 2020).

3. Results

3.1. Refractive indices and densities

A reference value of the refractive index of each of our ices was needed to measure ice thicknesses, which in turn were needed to determine absorption coefficients, band strengths, and optical constants. Calculations of the IR band strengths of an ice also required the ice's density. For the present study, the refractive index at 670 nm (n_{670}) and density (ρ) of both crystalline and non-crystalline C_3H_8, C_3H_6, and C_3H_4 ices were measured in a UHV chamber (~10^{-10} Torr) with checks on n_{670} in an older vacuum system (~10^{-8} Torr). Working with the UHV system was more expensive and slower than working with the older vacuum chamber, and little difference was found in the values of n_{670} obtained. However, the UHV system had the great advantage of giving density values of ices. Such measurements of n_{670} and ρ for ices have been described in several publications, and in principle are straightforward albeit somewhat tedious. See Hudson et al. (2017) for more information, and Romanescu et al. (2010) and Luna et al. (2012) for examples from other laboratories.

Table 1 summarizes our measurements of the refractive index at 670 nm and density of crystalline and non-crystalline C_3H_8, C_3H_6, and C_3H_4 ices. Uncertainties (standard errors) are on the order of ±0.005 and ± 0.005 g cm^{-3} for n_{670} and ρ, respectively. Density values are given only for the high-temperature stable crystalline phase of each ice investigated. Differences in ρ among crystalline phases of each compound are expected to be only a few percent based on previous work with crystalline phases of CH_3CN (Enjalbert and Galy, 2002), CH_3OH (Torrie et al., 2002), CH_4 (Bol'shutkin et al., 1971) and H_2O, I_c and I_h (Loerting et al., 2011).

Table 1
Refractive indices and densities of three hydrocarbon ices[a].

Form	Propane, C_3H_8		Propylene, C_3H_6		Propyne, C_3H_4	
	n	ρ/g cm^{-3}	n	ρ/g cm^{-3}	n	ρ/g cm^{-3}
Amorphous	1.357 (15 K)	0.653 (15 K)	1.384 (15 K)	0.663 (15 K)	1.370 (15 K)	0.705 (15 K)
Crystalline	1.484 (65 K)	0.797 (65 K)	1.445 (65 K)	0.782 (65 K)	1.533 (80 K)	0.866 (80 K)

[a] Values of n and ρ are averages of at least three measurements.

3.2. Propane - infrared spectra

When we began this study of C_3 hydrocarbons, we were unable to find many publications, other than spectroscopic work, on solid propane or solid propylene. Two papers were particularly suggestive. First, Pavese and Besley (1981) identified two solid phases on cooling liquid propane, with one phase being substantially more stable than the other. Second, differential thermal analyses of both propane and propylene by Takeda et al. (1990), starting with a vapor-deposited amorphous solid in each case, clearly identified two crystallizations for each compound, each well below the sample's melting point. Combined with our earlier study (Hudson et al., 2014b) of the next smaller alkane and alkene (i.e., ethane and ethylene) and the two crystalline phases of each, we suspected that two crystalline phases might also be found in the present work on propane and propylene, and such was the case.

Infrared survey spectra of solid propane (C_3H_8) are shown in Fig. 1. The sample giving the spectrum in (a) was made by vapor-phase deposition onto a substrate at 8 K under conditions that ensured that the resulting ice was amorphous in form. Warming to 40 K had little effect on the IR spectrum, but substantial irreversible changes took place on warming to 50 K, followed by equally distinct irreversible changes on going to 60 K. The survey spectra of Fig. 1 are useful for quickly seeing the relative intensities of IR peaks at these different temperatures over a broad range, but more details are seen in the expansions of Figs. 2–4 for the 3000–2800, 1500–1300, and 1200–700 cm^{-1} regions, respectively.

The sharpening, splitting, and shifts of propane's IR features on warming from 40 to 50 K are all signs of the amorphous ice's crystallization. The additional changes seen at 60 K suggest that a second phase change occurred, a crystalline-crystalline transition. Repeated warming and cooling failed to reverse either change. For convenience, we refer to the crystalline ice first encountered on warming as phase I and the second crystalline ice met as phase II. Slow cooling of the phase II ice from ~60 K and higher to the 50–60 K region did not reconvert it into the phase I solid.

Positions of selected spectral peaks of our propane ices are given in Tables 2–4. Also included in these tables are approximate assignments and descriptions for peaks and vibrational modes, respectively. In most cases, these descriptions are highly simplified, as can be seen from Gough et al. (1987), which should be consulted for potential energy distributions and additional references. In our section 4.2 we return to Table 3's "metastable" label. Smaller mid-IR spectral features, such as overtone and combination peaks, were seen, but not studied.

In addition to the warming sequence from 8 K in Figs. 1–4, propane was deposited at various temperatures up to ~80 K. Deposition near 50 K gave the spectrum of the phase I ice, deposition at 60 K gave the phase II form, and deposition at 55 K gave a mixture of the two. The spectra of ices deposited at these particular temperatures were essentially the same as those made by depositing near 8 K and warming.

We also found that for propane ices with thicknesses of a few

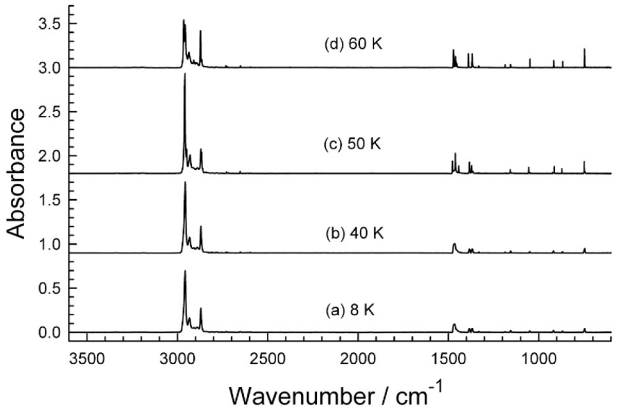

Fig. 1. Mid-IR survey spectra of C_3H_8 deposited at 8 K and warmed to the temperatures indicated. Spectra are offset for clarity. Spectra (a) and (b) are for amorphous propane, while (b) and (c) are for metastable (phase I) and stable (phase II) crystalline propane. See the text for details.

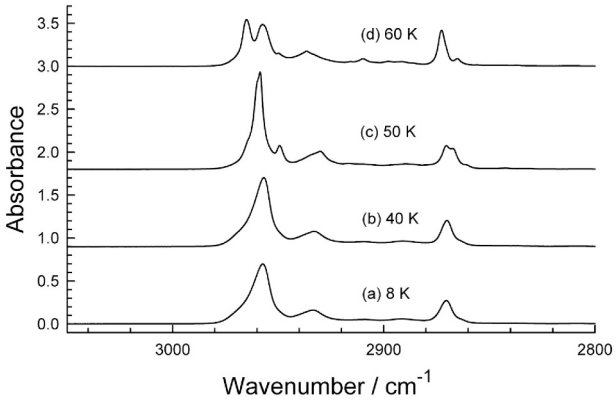

Fig. 2. Mid-IR spectra of C_3H_8 deposited at 8 K and warmed to the temperatures indicated. Spectra are offset for clarity. Spectra (a) and (b) are for amorphous propane, while (b) and (c) are for metastable (phase I) and stable (phase II) crystalline propane. See the text for details.

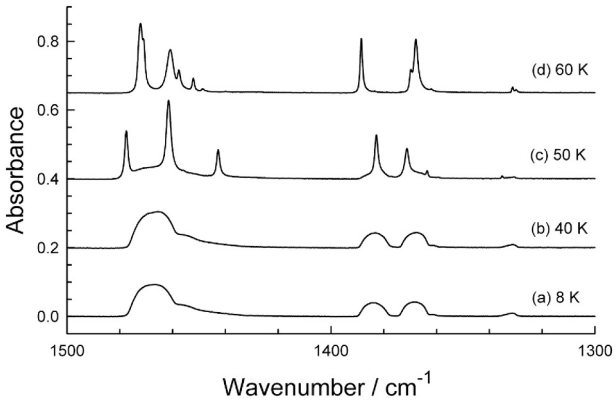

Fig. 3. Mid-IR spectra of C_3H_8 deposited at 8 K and warmed to the temperatures indicated. Spectra are offset for clarity. Spectra (a) and (b) are for amorphous propane, while (b) and (c) are for metastable (phase I) and stable (phase II) crystalline propane. See the text for details.

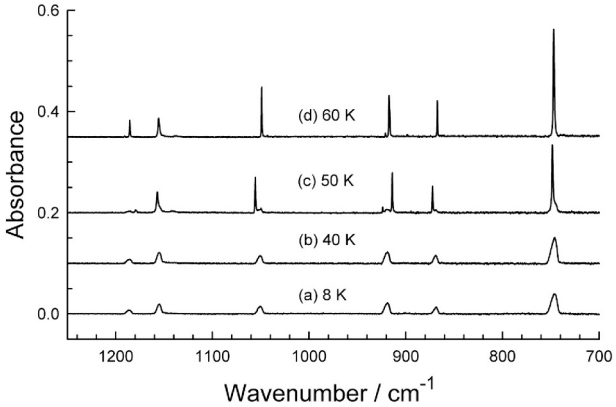

Fig. 4. Mid-IR spectra of C_3H_8 deposited at 8 K and warmed to the temperatures indicated. Spectra are offset for clarity. Spectra (a) and (b) are for amorphous propane, while (b) and (c) are for metastable (phase I) and stable (phase II) crystalline propane. See the text for details.

Table 2
Positions and intensities of selected IR features of amorphous C_3H_8 at 8 K.

Approximate description[a]	$\tilde{\nu}$/cm^{-1}	α'/cm^{-1}	Integration range/cm^{-1}	A' / 10^{-18} cm molecule^{-1}
CH stretches	2957	18,000	3000–2850	44.6
CH stretches	2870	6980		
CH_3, CH_2 scissoring	1466	2220	1500–1410	4.70
CH_3 CH wagging (in phase)	1384	943	1393–1375	0.881
CH_3 CH wagging (out of phase)	1368	954	1375–1355	0.906
CH_2 CH wagging	1331	189	1340–1325	0.0840
CH_3/CH_2 rocking	1186	164	1195–1180	0.101
CH_3 wagging, deformation	1155	436	1165–1140	0.278
C-C a-stretching	1051	324	1060–1040	0.213
CH_3 CCH deformation	919	484	930–908	0.331
C-C s-stretching	869	319	880–860	0.178
CH_2, CH_3 twisting, rocking	746	975	755–735	0.816

[a] Approximate descriptions are taken from Gough et al. (1987) and references therein; a = antisymmetric; s = symmetric.

Table 3
Positions and intensities of selected IR features of metastable crystalline C_3H_8 at 50 K.

Approximate description[a]	$\tilde{\nu}$ / cm^{-1}	α' / cm^{-1}	Integration range / cm^{-1}	A' / 10^{-18} cm molecule^{-1}
CH stretches	2958	20,800	3000–2800	36.3
CH stretches	2870	6620		
CH_3, CH_2 scissoring	1462	2900	1500–1400	3.81
CH_3 CH wagging (in phase)	1383	1710	1393–1375	0.662
CH_3 CH wagging (out of phase)	1371	1260	1375–1355	0.672
CH_2 CH wagging	1331	159	1340–1325	0.054
CH_3/CH_2 rocking	1185	113	1193–1180	0.045
CH_3 wagging, deformation	1157	616	1165–1145	0.238
C-C a-stretching	1056	713	1060–1045	0.203
CH_3 CCH deformation	914	812	925–910	0.306
C-C s-stretching	872	576	875–860	0.165
CH_2, CH_3 twisting, rocking	748	1760	760–735	0.786

[a] Approximate descriptions are taken from Gough et al. (1987) and references therein; a = antisymmetric; s = symmetric.

micrometers, it was possible to warm them above propane's melting point of ~85 K and to record the IR spectrum of the resulting liquid before its complete evaporation, which typically was only a few minutes. Liquid-phase spectra are not shown here, but resembled those of amorphous propane, as expected. Perhaps more significant is that on cooling liquid propane, the ice that formed was always in the crystalline phase-II form. Repeated warmings of such crystalline ices gave a melting point between 85.5 and 85.9 K, in agreement with the literature (Pavese and Besley, 1981). In a few cases, supercooling of liquid propane was observed, in one case as low as 78 K. The tendency of both propane and propylene to undergo supercooling has been known for about a century, and perhaps longer (Maass and Wright, 1921).

3.3. Propane - infrared intensities

Before continuing we should mention previous IR studies of solid propane. An older paper of Snyder and Schachtschenider (1963) listed peak positions at 1500–700 cm^{-1} for a propane ice at 77 K, which are close to those of our phase II solid, although the authors describe their sample as "a very viscous liquid" and the relative intensities of their

Table 4
Positions and intensities of selected IR features of stable crystalline C_3H_8 at 65 K.

Approximate description[a]	$\tilde{\nu}$/cm^{-1}	α'/cm^{-1}	Integration range/cm^{-1}	A'/10^{-18} cm molecule^{-1}
CH stretches	2957	6020	3000–2800	18.7
CH stretches	2872	4470		
CH_3, CH_2 scissoring	1472	2860	1500–1400	1.81
CH_3 CH wagging (in phase)	1388	2180	1393–1375	0.315
CH_3 CH wagging (out of phase)	1368	1710	1375–1355	0.474
CH_2 CH wagging	1331	164	1340–1325	0.0163
CH_3/CH_2 rocking	1185	542	1190–1180	0.0489
CH_3 wagging, deformation	1156	522	1165–1145	0.107
C-C a-stretching	1049	989	1052–1046	0.0851
CH_3 CCH deformation	917	843	920–914	0.0907
C-C s-stretching	867	1040	870–865	0.0765
CH_2, CH_3 twisting, rocking	746	3510	752–742	0.534

[a] Approximate descriptions are taken from Gough et al. (1987) and references therein; a = antisymmetric; s = symmetric.

spectrum's peaks do not match ours. A publication by Goodman et al. (1983) included a spectrum and a list of peak positions for crystalline propane at 77 K. Their spectrum covered only the 1400 to 700 cm^{-1} region, but their peaks' positions, spacings, and relative intensities suggest that the authors made the phase II form of crystalline propane. Coustenis et al. (1999) showed an IR spectrum of solid propane at 80 K, which also appears to correspond to our phase II ice. Much more recently, Ghosh et al. (2018) published IR spectra of solid propane similar to our own, but their spectra were collected in a reflection mode preventing a direct comparison of peak positions and intensities to our work (e.g., Maeda and Schatz, 1961). Nevertheless, it is clear that those authors found the same three solid forms we observed and at comparable temperatures. We will return to their paper in our Discussion section.

Our point here is simply to emphasize that none of the earlier papers provided quantitative measures of IR spectral intensities for solid propane, an important motivation for our investigation. In response, we prepared ice samples of various thicknesses for amorphous and crystalline propane and recorded their transmission IR spectra. The usual Beer's Law graphs gave values of the apparent absorption coefficient (α') and apparent band strengths (A') for selected peaks and regions, all of which are summarized in Tables 2-4.

3.4. Propylene - infrared spectra and infrared intensities

Our work with propylene followed the pattern just described for propane. In Fig. 5, mid-IR survey spectra for propylene are shown for four temperatures, with expansions in Figs. 6-8. Going from the bottom to the top, traces (a) and (b) are from an amorphous propylene sample made at 9 K and then warmed to 60 K. Trace (c) shows sharpening, shifting, and splitting of peaks on crystallization of the ice by 70 K, followed by a second crystallization for spectrum (d) at 80 K. Each crystallization was complete at these temperatures in about 1 min, but could be accomplished by holding the sample at lower temperatures for longer times. Such changes, as with propane, were never reversed on recooling the ice. Again as with propane, it was possible to warm propylene to its melting point near 87 K and to record IR spectra of the resulting liquid as it evaporated, which occurred in only a few minutes. Such spectra resembled those in trace (a) of Figs. 5-8, as expected. No attempt was made to narrow down the temperature ranges for crystallizations and other changes, nor to investigate the kinetics of such processes.

The behavior of amorphous propylene on warming differed somewhat from that of amorphous propane. The warming of propylene from

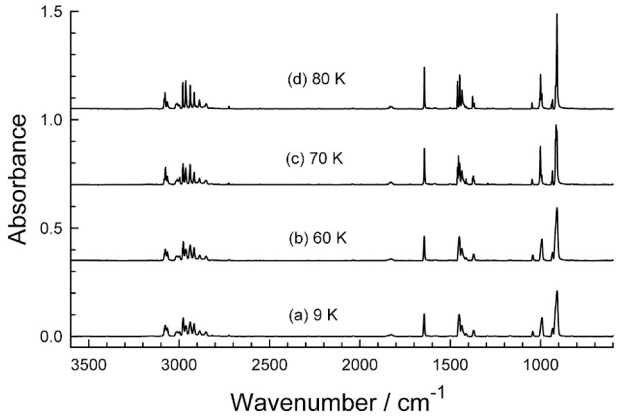

Fig. 5. Mid-IR survey spectra of C_3H_6 deposited at 9 K and warmed to the temperatures indicated. Spectra are offset for clarity. Spectra (a) and (b) are for amorphous propylene, while (b) and (c) are for metastable (phase I) and stable (phase II) crystalline propylene. See the text for details.

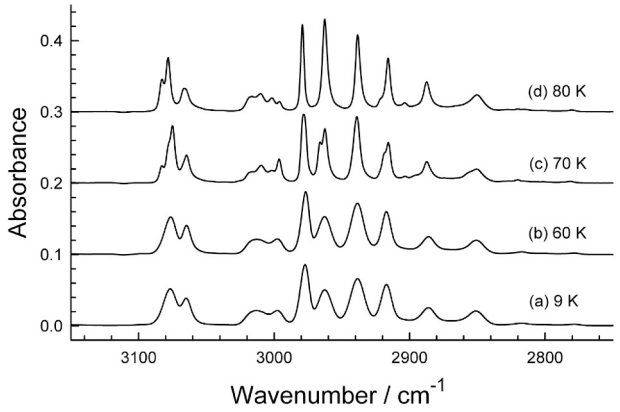

Fig. 6. Mid-IR spectra of C_3H_6 deposited at 9 K and warmed to the temperatures indicated. Spectra are offset for clarity. Spectra (a) and (b) are for amorphous propylene, while (b) and (c) are for metastable (phase I) and stable (phase II) crystalline propylene. See the text for details.

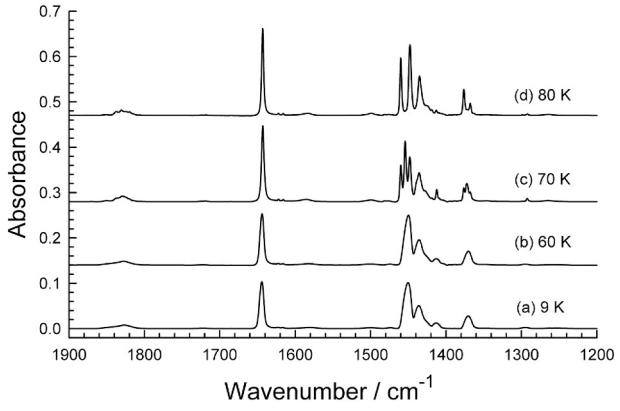

Fig. 7. Mid-IR spectra of C_3H_6 deposited at 9 K and warmed to the temperatures indicated. Spectra are offset for clarity. Spectra (a) and (b) are for amorphous propylene, while (b) and (c) are for metastable (phase I) and stable (phase II) crystalline propylene. See the text for details.

~9 K typically gave a mixture of two crystalline forms near 70 K, which evolved into a single crystalline form by 80 K. This can be seen upon close inspection of Figs. 5–8, but is much easier to see in the expansion of

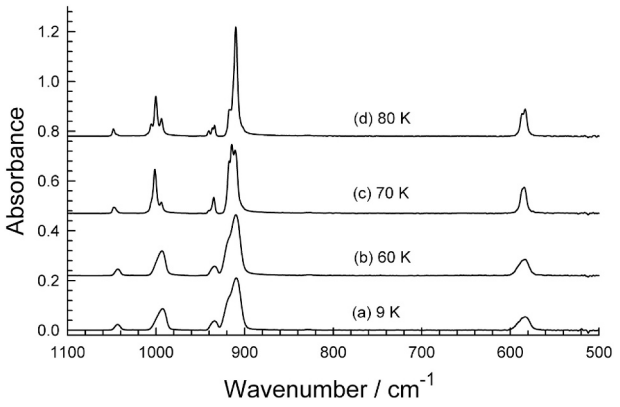

Fig. 8. Mid-IR spectra of C_3H_6 deposited at 9 K and warmed to the temperatures indicated. Spectra are offset for clarity. Spectra (a) and (b) are for amorphous propylene, while (b) and (c) are for metastable (phase I) and stable (phase II) crystalline propylene. See the text for details.

Fig. 9. Trace (a) is a typical result, obtained on warming propylene from 8 to 70 K. Further warming gave spectrum (b) at 80 K, which could be subtracted from (a) to give the difference spectrum (c). That this represents a single crystalline form is supported by trace (d), obtained on deposition of propylene at 75 K to give a crystalline phase-I ice spectrum. In short, the warming of amorphous propylene often gave a mixture of the two crystalline phases. We did not investigate all of the factors involved, but we did determine that deposition at ~70 K consistently gave the phase I ice and deposition at ~80 K always gave the phase II ice, and these were the conditions used to prepare samples for intensity measurements.

Tables 5–7 give peak positions for our three forms of solid propylene, along with assignments and descriptions for IR peaks and vibrational modes, respectively. As with the case of propane, in most instances these descriptions are highly simplified. See Silvi et al. (1973) for more information, such as potential energy distributions and additional references. Infrared intensities for solid propylene, both absorption coefficients and band strengths, again were determined from the appropriate Beer's Law plots. See Tables 5–7 for results.

3.5. *Propyne - infrared spectra and infrared intensities*

Our propyne work followed the pattern already described for propane and propylene, but proved to be somewhat simpler as only one crystalline phase was found. In Figs. 10–13, mid-IR survey spectra for propyne are shown for three temperatures. Going from the bottom to the top, traces (a) and (b) are from an amorphous propyne sample made at

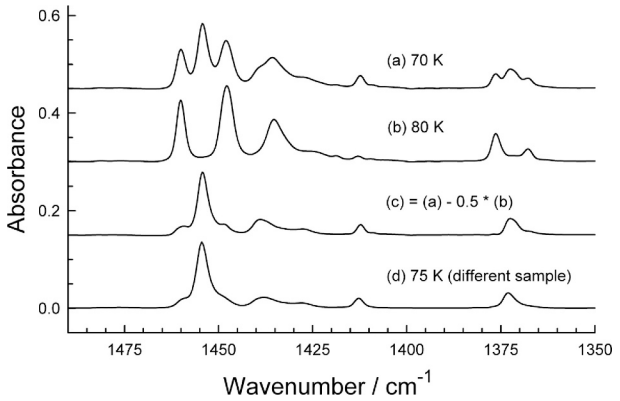

Fig. 9. Mid-IR spectra of C_3H_6 deposited at 9 K and warmed to (a) 70 K and then to (b) 80 K. Trace (c) is a difference spectrum and trace (d) is for a propylene ice made at 75 K. Spectra are offset for clarity.

Table 5
Positions and intensities of selected IR features of amorphous C_3H_6 at 8 K.

Approximate description[a]	$\tilde{\nu}$/cm^{-1}	α'/cm^{-1}	Integration range/cm^{-1}	A'/10^{-18} cm molecule^{-1}
CH_2 a-stretches	3077	1220	3120–3040	2.44
CH_2 s-stretches	2977	2070	3040–2750	10.7
CH_3 a-stretches	2938	1600		
CH_3 s-stretches	2917	1250		
C=C stretch	1644	2300	1660–1630	1.69
CH_3 a-bending	1450	2210	1466–1400	4.44
CH_3 s-bending	1370	587	1385–1355	0.657
CH_3 wagging	1043	457	1055–1030	0.385
CH bending	993	1798	1015–975	2.40
CH_2 bending/C—C stretching	909	4250	950–880	8.33
C-CH_2 twisting	585	871	610–565	1.35

[a] Approximate descriptions are taken from Silvi et al. (1973) and references therein; a = antisymmetric; s = symmetric.

Table 6
Positions and intensities of selected IR features of metastable crystalline C_3H_6 at 65 K.

Approximate description[a]	$\tilde{\nu}$/cm^{-1}	α'/cm^{-1}	Integration range/cm^{-1}	A'/10^{-18} cm molecule^{-1}
CH_2 a-stretches	3075	4580	3110–3040	2.42
CH_2 s-stretches	2977	4860	3040–2750	8.12
CH_3 a-stretches	2940	3270		
CH_3 s-stretches	2919	1790		
C=C stretch	1641	3220	1660–1625	1.91
CH_3 a-bending	1454	9030	1466–1400	4.78
CH_3 s-bending	1371	2040	1385–1355	0.747
CH_3 wagging	1046	996	1055–1030	0.366
CH bending	1002	6640	1015–975	2.70
CH_2 bending/C—C stretching	914	13,600	950–880	7.80
C-CH_2 twisting	585	2550	610–565	1.57

[a] Approximate descriptions are taken from Silvi et al. (1973) and references therein; a = antisymmetric; s = symmetric.

Table 7
Positions and intensities of selected IR features of stable crystalline C_3H_6 at 80 K.

Approximate description[a]	$\tilde{\nu}$ cm^{-1}	α'/cm^{-1}	Integration range/cm^{-1}	A'/10^{-18} cm molecule^{-1}
CH_2 a-stretches	3078	1090	3100–3040	1.04
CH_2 s-stretches	2979	2990	3040–2750	8.43
CH_3 a-stretches	2939	3750		
CH_3 s-stretches	2916	3100		
C=C stretch	1643	8750	1660–1625	2.33
CH_3 a-bending	1448	6050	1466–1400	5.26
CH_3 s-bending	1368	1310	1385–1355	0.586
CH_3 wagging	1048	1330	1055–1035	0.366
CH bending	1000	5410	1015–975	3.14
CH_2 bending/C—C stretching	909	10,200	950–880	8.27
C-CH_2 twisting	583	2730	610–565	2.38

[a] Approximate descriptions are taken from Silvi et al. (1973) and references therein; a = antisymmetric; s = symmetric.

8 K and then warmed to 60 K. Trace (c), for 70 K, shows a hint of change, which is complete in (d) by 80 K with peaks sharpening, shifting, and splitting on crystallization of the ice, changes that were never seen to reverse on recooling the sample. Tables 8 and 9 give peak positions for our two forms of solid propyne, along with assignments and descriptions for IR peaks and vibrational modes, respectively. As with propane and propylene, in most instances these descriptions are highly simplified. Peak assignments are from the gas-phase studies of Crawford Jr. (1940) and Whitmer (1974), which should be consulted for potential energy distributions and references to earlier work. Infrared intensities for solid

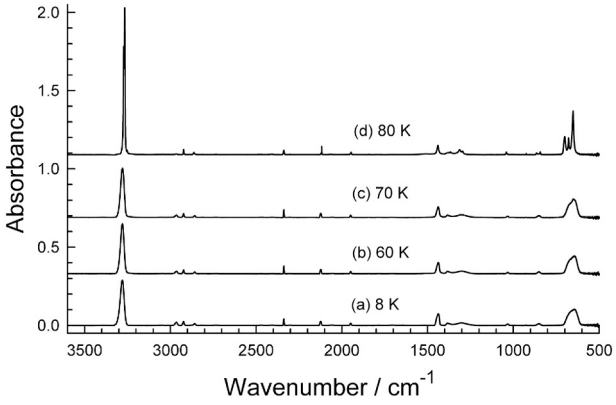

Fig. 10. Mid-IR survey spectra of C_3H_4 deposited at 8 K and warmed to the temperatures indicated. Spectra are offset for clarity. Spectra (a), (b), and (c) are for amorphous propyne, while (d) is for crystalline propyne. See the text for details.

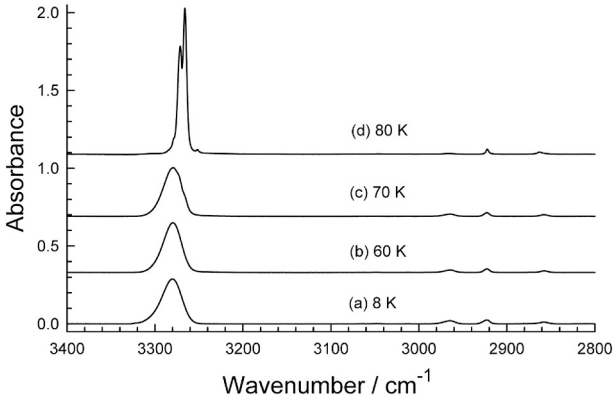

Fig. 11. Mid-IR spectra of C_3H_4 deposited at 8 K and warmed to the temperatures indicated. Spectra are offset for clarity. Spectra (a), (b), and (c) are for amorphous propyne, while (d) is for crystalline propyne. See the text for details.

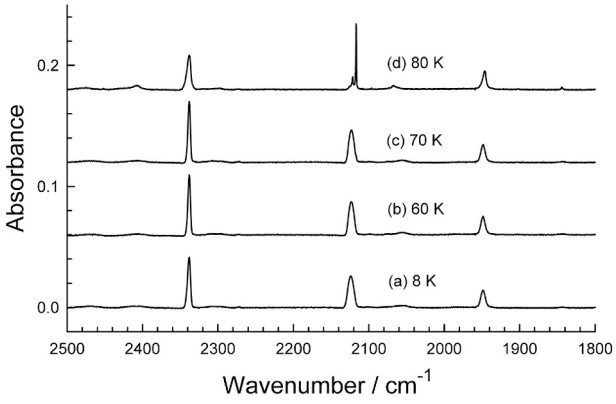

Fig. 12. Mid-IR spectra of C_3H_4 deposited at 8 K and warmed to the temperatures indicated. Spectra are offset for clarity. Spectra (a), (b), and (c) are for amorphous propyne, while (d) is for crystalline propyne. See the text for details.

propyne, both absorption coefficients and band strengths, again were determined from the appropriate Beer's Law plots. See Tables 8 and 9 for results. Finally, our amorphous-propyne spectra showed small peaks for contamination by ~0.1% CO_2 (2338 cm^{-1}) and ~ 1% allene (1948 cm^{-1}). Our estimate for the abundance of propyne's isomer allene (1,2-propadiene) is expected to decrease after a more-precise

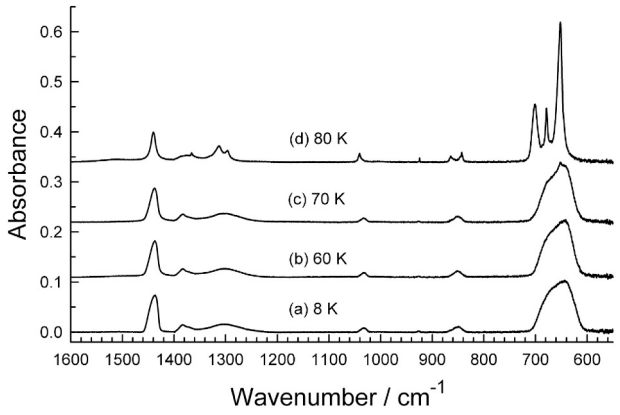

Fig. 13. Mid-IR spectra of C_3H_4 deposited at 8 K and warmed to the temperatures indicated. Spectra are offset for clarity. Spectra (a), (b), and (c) are for amorphous propyne, while (d) is for crystalline propyne. See the text for details.

Table 8
Positions and intensities of selected IR features of amorphous C_3H_4 at 8 K.

Approximate description[a]	$\tilde{\nu}$/cm^{-1}	α'/cm^{-1}	Integration range/cm^{-1}	A'/10^{-18} cm molecule^{-1}
H-C≡ stretches	3280	6430	3333–3233	17.7
C≡C stretch	2124	540	2136–2112	0.469
C-H bending	1437	1570	1462–1414	2.87
H-C≡C bending	645	2190	720–590	13.3

[a] Approximate descriptions are from Crawford Jr. (1940) and Whitmer (1974).

Table 9
Positions and intensities of selected IR features of crystalline C_3H_4 at 80 K.

Approximate description[a]	$\tilde{\nu}$/cm^{-1}	α'/cm^{-1}	Integration range/cm^{-1}	A'/10^{-18} cm molecule^{-1}
H-C≡ stretches	3266	54,100	3290–3240	29.1
C≡C stretch	2117	3820	2119–2114	0.197
C-H bending	1441	1970	1460–1410	1.10
H-C≡C bending	700	8220	720–660	9.84
H-C≡C bending	678	9270		

[a] Approximate descriptions are from Crawford Jr. (1940) and Whitmer (1974).

determination of allene's IR band strengths, which is work in progress. No work was done above about 90 K due to propyne's sublimation in our vacuum system.

3.6. Optical constants

We also have calculated IR optical constants *n* and *k* for the amorphous and crystalline forms of propane, propylene, and propyne. See Fig. 14 for the stable crystalline form of propane. Electronic versions of these optical constants are posted on our group's website (https://science.gsfc.nasa.gov/691/cosmicice/constants.html). From these numbers it is possible to calculate, among other things, IR transmission spectra for ices of various thicknesses, as well as reflection spectra. See Swanepoel (1983) for a simple method for calculating spectra from optical constants. For a method to calculate IR reflection spectra from *n* and *k* see Tomlin (1968).

4. Discussion

4.1. Propane, propylene, and propyne IR spectra

The IR spectra of propane in Figs. 1-4 are about as expected based on

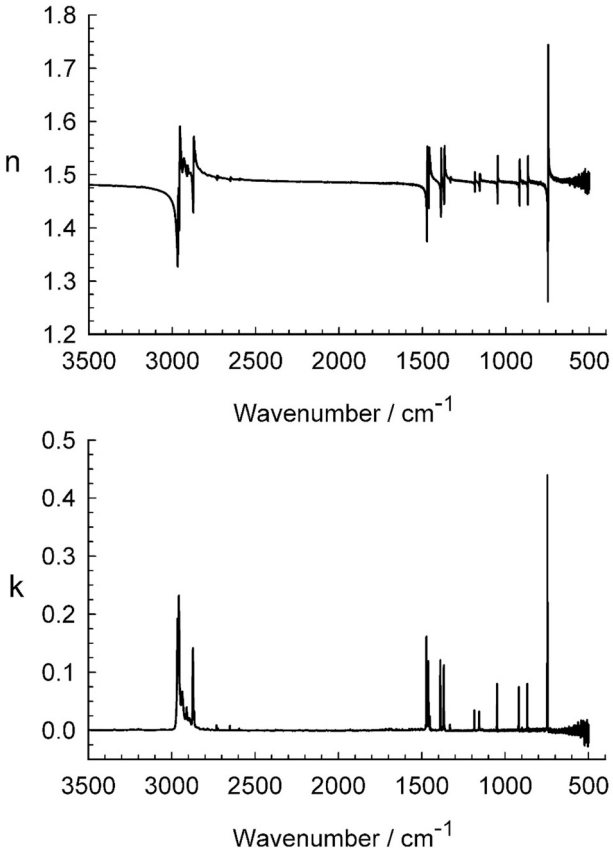

Fig. 14. Optical constants of the stable crystalline form of propane at 80 K.

the literature already cited. Lab-to-lab variations make quantitative comparisons of intensities difficult, but our peak positions for propane are in reasonable agreement with earlier work, allowing for differences in temperature, sample preparation, and so on. The propane results that are closest to our own are those of Ghosh et al. (2018). Their paper's IR spectra show only the ~3000–2830 and 1520–1320 cm^{-1} regions, but there is close agreement with our Figs. 2 and 3. However, since the spectra of Ghosh et al. were recorded by reflection off a metal substrate, which can alter relative intensities, a more direct comparison is difficult (e.g., Pacansky and England, 1986). Seen that way, our Figs. 1–4 appear to be the first IR transmission spectra of these forms of solid propane, all recorded from a single sample, and our Table 3 appears to be the first tabulation of peak positions of the metastable crystalline form of solid propane.

Comments similar to these also apply to our IR results for propylene ices. We are unaware of previous work showing spectra of the three solid phases reported here, all recorded in transmission with quantitative measurements of band and peak intensities. Moreover, we are unaware of any spectra of the metastable crystalline phase of propylene other than those presented here.

As with its smaller alkyne relation, acetylene (HC≡CH), propyne displayed only amorphous and crystalline solid forms (Hudson et al., 2014a). Unlike the cases of the two other C_3 compounds in this paper, we were unable to find previous spectra of solid propyne covering the full mid-IR region. The liquid-phase Raman spectrum of Crawford Jr. (1940) bears some similarities to our infrared spectra, but comparisons are difficult other than for peak positions.

4.2. Propane, propylene, and propyne ices

Our observation of the formation of amorphous ices on slow deposition at cryogenic temperatures certainly is not new (Malherbe and

Bernstein, 1951; Nightingale and Wagner, 1954). Our spectra of amorphous hydrocarbons show the usual characteristics, namely broad IR features resembling those of a liquid, and with peaks that sharpen, split, and shift when crystallization takes place on warming. As already mentioned, no difficulty was met in making amorphous forms of these C_3 hydrocarbons, unlike with some C_2 hydrocarbons in our earlier work (e.g., Hudson et al., 2014a; Hudson et al., 2014b).

The situation with our crystalline hydrocarbon ices is more complicated, with two crystalline phases being observed for both propane and propylene. In our studies of CH_3CN and CH_3SH, two crystalline forms were expected and found for each compound, and our identifications of each phase were considerably helped by prior diffraction and spectroscopic results (Hudson, 2016; Hudson, 2020). Unfortunately, we have not found similar studies of either propane or propylene. The best we can do for our hydrocarbons' stable crystalline phases is again to note that the form we have labeled as crystalline phase II in each case was never seen to convert into the crystalline phase I form. Moreover, on heating propane and propylene ices until they melted and then recooling them, IR spectra of the phase II form were always obtained. These observations suggest that what we have designated as the phase II polymorphs of propane and propylene are indeed the stable forms at the temperatures indicated. These conclusions place our work in agreement with that of Ghosh et al. (2018). We also are in agreement with the earlier calorimetric study of Takeda et al. (1990) of the irreversible formation of two phases on warming amorphous propane and amorphous propylene.

In contrast, the situation with our metastable crystalline phase I forms is less clear, except that they convert into the phase II structures on warming. Returning again to our earlier studies, we found that warming amorphous CH_3CN produced first the kinetically favored high-temperature crystalline phase of acetonitrile and not the thermodynamically and perhaps intuitively favored low-temperature phase, in agreement with the Ostwald step rule (Ostwald, 1897; Tizek et al., 2004). Here we suggest that amorphous propane and amorphous propylene might behave in a similar manner. What we have described as metastable hydrocarbon solids (phase I) forming on crystallization from amorphous ices, followed by stable forms (phase II) on additional warming, could be the result of a competition between kinetic and thermodynamic control as seen with amorphous CH_3CN and CH_3SH ices (Hudson, 2016; Hudson, 2020). Our IR results seem consistent with that as trace (c) in Fig. 2, for the metastable form (phase I) of propane, appears to more closely resemble the disordered amorphous-ice spectra of (a) and (b) than does trace (d) for phase II.

We also suggest that the adjectives "metastable" and "stable" for phases I and II, respectively, might need to be exchanged at higher temperatures, such as in a narrow region near the melting points of propane and propylene. This interpretation could also help reconcile the work of Pavese and Besley (1981), of two crystalline forms of propane near the compound's melting point, with the results presented here and by Takeda et al. (1990), and Ghosh et al. (2018). We and the latter two groups approached propane crystallization by warming an amorphous solid, but Pavese and Besley (1981) studied crystallization by starting with room-temperature liquid propane, also an amorphous material. Although it is difficult to compare stabilities and temperatures for solid-solid transitions between these two types of experiments, we suggest that our phases I and II might well correspond to phases β and α, respectively, of Pavese and Besley (1981), the differences in stability in the two types of experiment being due to differences in temperature and mode of formation.

Clearly, further study is needed to clarify this situation. Boese et al. (1999) summarized the results of earlier work on the next higher (i.e., butane) and lower (i.e., ethane) alkanes from propane, noting that an orientationally disordered phase of each exists just below the compound's melting point. Such may well be true of propane too.

Comments similar to those just made for propane's phases also apply to propylene. We know of no comparable work on solid propylene other than that already mentioned. It is interesting that both we and Takeda et al. (1990, 1991) find that crystallization of amorphous propane occurs on the order of 10 K lower than for amorphous propylene. Propane's symmetrical (H_3C-CH_2-CH_3) arrangement of two C—C single bonds about the central carbon suggests that the formation of a crystalline structure might well be more facile than for propylene (H_2C=CH-CH_3), with a specific arrangement of C—C and C=C bonds needed to make a crystal. It would be interesting to test this interpretation by measuring the temperature regions for crystallization of amorphous propyne (HC ≡ C-CH_3) and its more-symmetrical isomer allene (H_2C=C=CH_2). We predict that allene crystallization will occur at lower temperatures than for propyne.

4.3. Applications and extensions

The applications of our work are primarily to extraterrestrial environments at temperatures below about 90 K. The amorphous forms of our pure hydrocarbons will be those expected at the lower temperatures, especially if, as is likely, these compounds are combined with more abundant materials. Our crystalline ices would seem to have less application, except perhaps to cases such as Titan where temperatures would permit crystallization. Hydrocarbon clouds dominated by methane (CH_4) and subject to magnetospheric bombardment, will produce more-complex hydrocarbons, including those examined here, and some will be at temperatures expected to lead to propane, propylene, and propyne ices.

We also should mention extensions of our results to other spectral regions. There are planetary-science observations that employ the near-IR region and interstellar work that uses far-IR wavelengths. Our mid-IR results sit in the middle of these two regions. The mid-IR band absorption coefficients and band strengths in our tables can readily be used as reference data to scale near- or far-IR spectral features and obtain intensity data for those regions. See Gerakines et al. (2005) and Giulano et al. (2014) for two examples.

Laboratory applications also are readily envisioned. Low-temperature in situ radiolysis work has been reported for the simpler hydrocarbons methane and ethane, and the formation of more-complex hydrocarbons has been found by IR spectroscopy. The data reported here allow for the first accurate quantification of such low-temperature results, such as determinations of reaction yields and branching ratios. Simple photolytic or radiolytic oxidations (hydrogen loss) such as $C_3H_8 \rightarrow C_3H_6 \rightarrow C_3H_4$ can now be quantified. Conversely, starting with the simplest of these three hydrocarbons one can now quantify reductions such as $C_3H_4 \rightarrow C_3H_6 \rightarrow C_3H_8$ as well as conversions of C_3H_4 and C_3H_6 to make 3-carbon alcohols (e.g., Qasim et al., 2019).

As for needs, several already have been mentioned. Certainly diffraction studies are needed for the solid phases of these compounds as are studies of the IR spectra in closed cells. It also would be useful to have better data on the IR spectra of the liquid forms of our hydrocarbons, and the degree to which supercooling can be detected remotely in the laboratory and on planetary surfaces. Our results also could be used to determine vapor pressures for our compounds, and perhaps enthalpies of sublimation (Khanna et al., 1990). Quantitative extensions of our spectral measurements to both shorter and longer wavelengths are needed, and should be straightforward now that our IR intensity data are available. Also, our optical constants will permit spectral simulations of hydrocarbon particles, such as in hazes, with variations in particle shape and size. Finally, the somewhat surprising formation and stability of liquid propane and liquid propylene in the 80 K region could open up new possibilities for liquid-phase measurements on these compounds of relevance to Titan, such as anticipating and interpreting results of NASA's Dragonfly mission. Given the complexity and costs of planetary missions, laboratory studies will continue to play a role in unraveling Solar System chemistry.

Declaration of Competing Interest

None.

Acknowledgments

NASA funding through the Cassini Data Analysis Program is acknowledged, as is support from NASA's Planetary Science Division Internal Scientist Funding Program through the Fundamental Laboratory Research (FLaRe) work package at the NASA Goddard Space Flight Center. YYY thanks the NASA Postdoctoral Program for her fellowship. Marla Moore (NASA, retired), Robert Ferrante (US Naval Academy), and Mark Loeffler (Northern Arizona University) contributed to various stages of this work.

References

Baratta, G.A., Domingo, M., Ferini, G., Leto, G., Palumbo, M.E., Satorre, M.A., Strazzulla, G., 2003. Ion irradiation of CH_4-containing icy mixtures. Nucl. Instru. Meth. Phys. Res. B 209, 283–287.
Behmard, A., Fayolle, E.C., Graninger, D.M., Bergner, J.B., Martín-Doménech, R., Maksyutenko, P., Rajappan, M., Öberg, K.I., 2019. Desorption kinetics and binding energies of small hydrocarbons. Astrophys. J. 875, 1.
Bennett, C.J., Jamieson, C.S., Osamura, Y., Kaiser, R.I., 2006. Laboratory studies on the irradiation of methane in interstellar, cometary, and solar system ices. Astrophys. J. 653, 792–811.
Boese, R., Weiss, H., Bläser, D., 1999. The melting point alternation in the short-chain *n*-alkanes: single-crystal X-ray analyses of propane at 30 K and of *n*-butane to *n*-nonane at 90 K. Angew. Chem. Int. Ed. 38, 988–992.
Bohn, R.B., Sandford, S.A., Allamandola, L.J., Cruikshank, D.P., 1994. Infrared spectroscopy of triton and Pluto ice analogs: the case for saturated hydrocarbons. Icarus 111, 151–173.
Bol'shutkin, D.N., Gasan, V.M., Prokhvatilov, A.I., 1971. Temperature dependence of parameter of a methane crystal lattice in a temperature range from 11–70 degrees K. Zhurnal Strukturnoi Khimii 12, 734–736.
Brown, M.E., Schaller, E.L., Blake, G.A., 2015. Irradiation products on dwarf planet Makemake. Astron. J. 149, 1–6.
Coustenis, A., Schmitt, B., Khanna, R.K., Trotta, F., 1999. Plausible condensates in Titan's stratosphere from voyager infrared spectra. Planet. Sp. Sci. 47, 1305–1329.
Crawford Jr., B.L., 1940. Infra-red and Raman spectra of polyatomic molecules. XII. Methyl acetylene. J. Chem. Phys. 8, 526–531.
Cruikshank, D.P., Dalle Ore, C.M., Clark, R.N., Pendleton, Y.J., 2014. Aromatic and aliphatic organic materials on Iapetus: analysis of Cassini VIMS data. Icarus 233, 306–315.
Cruikshank, D.P., Grundy, W.M., DeMeo, F.E., Buie, M.W., et al., 2015. Icarus 246, 82–92.
Dartois, E., Chabot, M., Pino, T., Béro, K., Godard, M., Severin, D., Bender, M., Trautmann, C., 2017. Swift heavy ion irradiation of interstellar dust analogues - small carbonaceous species released by cosmic rays. Astron. Astrophys. 599, 1.
de Barros, A.L.F., Bordalo, V., Seperuelo Duarte, E., da Silveira, E.F., Domarack, A., Rothard, H., Boduch, P., 2011. Cosmic ray impact on astrophysical ices: laboratory studies on heavy ion irradiation of methane. Astron. Astrophys. 513, 1–9.
De Sanctis, M.C., Ammannito, E., McSween, H.Y., et al., 2017. Localized aliphatic organic material on the surface of Ceres. Science 355, 719–722.
Enjalbert, R., Galy, J., 2002. CH_3CN: X-ray structural investigation of a unique single crystal. $\beta \rightarrow \alpha$ phase transition and crystal structure. Acta Cryst B58, 1005–1010.
Fleury, B., Gudipati, M.S., Couturier-Tamburelli, I., Carrasco, N., 2019. Photoreactivity of condensed acetylene on titan aerosols analogues. Icarus 321, 358–366.
Gerakines, P.A., Hudson, R.L., 2020. A Modified Algorithm and Open-Source Computational Package for the Determination of Infrared Optical Constants Relevant to Astrophysics. Accepted for publication.
Gerakines, P.A., Schutte, W.A., Ehrenfreund, P., 1996. Ultraviolet processing of interstellar ice analogs. I. Pure ices. Astron. Astrophys. 312, 289–305.
Gerakines, P.A., Bray, J.J., Davis, A., Richey, C., 2005. The strengths of near-infrared absorption features relevant to interstellar and planetary ices. Astrophys. J. 620, 1140–1150.
Ghosh, J., Hariharan, A.K., Bhuin, R.G., Methikkalam, R.R.J., Pradeep, T., 2018. Propane and propane–water interactions: a study at cryogenic temperatures. Phys. Chem. Chem. Phys. 20, 1838–1847.
Giulano, B.M., Escribano, R.M., Martin-Doménech, R., Dartois, E., Muñoz Caro, G.M., 2014. Interstellar ice analogs: band strengths of H_2O, CO_2, CH_3OH, and NH_3 in the far-infrared region. Astron. Astrophys. 565, A108.
Goodman, M.A., Sweany, R.L., Flurry Jr., R.L., 1983. Infrared spectra of matrix-isolated, crystalline solid, and gas-phase C_3-C_6 n-alkanes. J. Phys. Chem. 87, 1753–1757.
Gough, K.M., Murphy, W.F., Raghavachari, K., 1987. The harmonic force field of propane. J. Chem. Phys. 87, 3332–3340.
Hollenberg, J.L., Dows, D.A., 1961. Measurement of absolute infrared absorption intensities in crystals. J. Chem. Phys. 34, 1061–1063.
Hudson, R.L., 2016. Infrared spectra and band strengths of CH_3SH, an interstellar molecule. Phys. Chem. Chem. Phys. 18, 25756–25763.
Hudson, R.L., 2020. Preparation, identification, and low-temperature infrared spectra of two elusive crystalline nitrile ices. Icarus 338, 113548.
Hudson, R.L., Moore, M.H., Raines, L.L., 2009. Ethane ices in the outer solar system: spectroscopy and chemistry. Icarus 203, 677–680.
Hudson, R.L., Ferrante, R.F., Moore, M.H., 2014a. Infrared spectra and optical constants of astronomical ices: I. Amorphous and crystalline acetylene. Icarus 228, 276–287.
Hudson, R.L., Gerakines, P.A., Moore, M.H., 2014b. Infrared spectra and optical constants of astronomical ices: II. Ethane and ethylene. Icarus 243, 147–148.
Hudson, R.L., Loeffler, M.J., Gerakines, P.A., 2017. Infrared spectra and band strengths of amorphous and crystalline N_2O. J. Chem. Phys. 146, 0243304.
Khanna, R.K., Allen Jr., J.E., Masterton, C.M., Zhao, G., 1990. Thin-film infrared spectroscopic method for low-temperature vapor-pressure measurement. J. Phys. Chem. 94, 440–442.
Lang, E.K., Knox, K.J., Signorell, R., 2013. Phase behavior of propane and n-pentane aerosol particles under conditions relevant to titan. Planet. Sp. Sci. 75, 56–68.
Loerting, T., Bauer, M., Kohl, I., Watschinger, K., Winkel, K., Mayer, E., 2011. Cryoflotation: densities of amorphous and crystalline ices. J. Phys. Chem. B 115, 14167–14175.
Luna, R., Satorre, M.Á., Domingo, M., Millán, C., Santonja, C., 2012. Density and refractive index of binary CH_4, N_2 and CO_2 ice mixtures. Icarus 221, 186–191.
Maass, O., Wright, C.H., 1921. Some physical properties of hydrocarbons containing two and three carbon atoms. J. Am. Chem. Soc. 43, 1011–1098.
Maeda, S., Schatz, P.N., 1961. Absolute infrared intensity measurements in thin films. J. Chem. Phys. 35, 1617–1620.
Maguire, W.C., Hanel, R.A., Jennings, Kunde, V.G., Samuelson, R.E., 1981. C_3H_8 and C_3H_4 in Titan's atmosphere. Nature 292, 683–686.
Malherbe, F.E., Bernstein, H.J., 1951. Infrared spectra of rapidly solidified vapors. J. Chem. Phys. 19, 1607–1608.
Marcelino, N., Cernicharo, J., Agúndez, M., Roueff, E., Gerin, M., Martín-Pintado, J., Mauersberger, R., Thum, C., 2007. Discovery of interstellar propylene (CH_2CHCH_3): missing links in interstellar gas-phase chemistry. Astrophys. J. 665, L127–L130.
Mejía, C.F., de Barros, A.L.F., Bordalo, V., da Silveira, E.F., Boduch, P., Domaracka, A., Rothard, H., 2013. Cosmic ray-ice interaction studied by radiolysis of 15 K methane ice with MeV O, Fe and Zn ions. MNRAS 433, 2368–2379.
Mizuno, Y., Kofu, M., Yamauro, O., 2016. X-ray diffraction study on simple molecular glasses created by low-temperature vapor deposition. J. Phys. Soc. Jpn. 85, 124602.
Moore, M.H., Hudson, R.L., 1998. Infrared study of ion-irradiated water-ice mixtures with hydrocarbons relevant to comets. Icarus 135, 518–527.
Nightingale, R.E., Wagner, E.L., 1954. The vibrational spectra and structure of solid hydroxylamine and deutero-hydroxylamine. J. Chem. Phys. 22, 203–208.
Nixon, C.A., Jennings, D.E., Bézard, B., Vinatier, S., Teanby, N.A., Sung, K., Ansty, T.M., Irwin, P.G.J., Gorius, N., Cottini, V., Coustenis, A., Flasar, F.M., 2013. Detection of propene in Titan's stratosphere. Astrophys. J. 776, L14.
Ostwald, W., 1897. Studien über die Bildung und Umwandlung fester Körper. Z. Phys. Chem. 22, 289–330.
Pacansky, J., England, C.D., 1986. Analysis of infrared specular reflection spectroscopy of rare-gas matrices. J. Chem. Phys. 90, 4499–4508.
Pavese, F., Besley, L.M., 1981. Triple-point temperature of propane: measurements on two solid-to-liquid transitions and one solid-to-solid transition. J. Chem. Thermo. 13, 1095–1104.
Qasim, D., Fedoseev, G., Lamberts, T., Chuang, K., He, J., Ioppolo, S., Kästner, J., Linnartz, H., 2019. Alcohols on the rocks: solid-state formation in a $H_3CC{\equiv}CH$ + OH cocktail under dark cloud conditions. ACS Earth Space Chem. 209, 986–999.
Raponi, A., Ciarniello, M., Capaccioni, F., et al., 2020. Infrared detection of aliphatic organics on a cometary nucleus. Nat. Astron. 4, 500–505.
Roe, H.G., Greathouse, T.K., Richter, M.J., Lacy, J.H., 2003. Propane on titan. Astrophys. J. 597, L65–L68.
Romanescu, C., Marschall, J., Kim, D., Khatiwada, A., Kalogerakis, K.S., 2010. Refractive index measurements of ammonia and hydrocarbon ices at 632.8 nm. Icarus 205, 695–701.
Sasaki, T., Kanno, A., Ishiguro, M., Kinoshita, D., Nakamura, R., 2005. Search for nonmethane hydrocarbons on Pluto. Astrophys. J. 618, L57–L60.
Sephton, M.A., Pillinger, C.T., Gilmour, I., 2001. Normal alkanes in meteorites: molecular $\delta^{13}C$ values indicate an origin by terrestrial contamination. Precambrian Res. 106, 45–58.
Silvi, B., Labarbe, P., Perchard, J.P., 1973. Spectres de vibration et coordonnées normales de quatre espèces isotopiques de propène. Spectrochim. Acta 29A, 263–276.
Snyder, L.E., Buhl, D., 1973. Interstellar methylacetylene and isocyanic acid. Nature Phys. Sci. 243, 45–56.
Snyder, R.G., Schachtschenider, J.H., 1963. Vibrational analysis of the n-paraffins – I assignments of infrared bands in the spectra of C_3H_8 through n-$C_{19}H_{40}$. Spectrochim. Acta 19, 85–116.
Strazzulla, G., Calcagno, L., Foti, G., 1984. Build up of carbonaceous material by fast protons on Pluto and triton. Astron. Astrophys. 140, 441–444.
Swanepoel, R., 1983. Determination of the thickness and optical constants of amorphous silicon. J. Phys. E: Sci. Instrum. 16, 1214–1222.
Takeda, K., Oguni, M., Suga, H., 1990. A DTA apparatus for vapour-deposited samples. Characterisation of some vapour-deposited hydrocarbons. Thermochim. Acta 158, 195–203.
Takeda, K., Oguni, M., Suga, H., 1991. Thermo-analytical study of vapor-deposited n-alkanes. J. Phys. Chem. Solids 52, 991–997.
Teanby, N.A., Irwin, P.G.J., de Kok, R., Jolly, A., Bézard, B., Nixon, C.A., Calcutt, S.B., 2009. Titan's stratospheric C2N2, C3H4, and C4H2 abundances from Cassini/CIRS far-infrared spectra. Icarus 202, 620–631.
Tempelmeyer, K.E., Mills, D.W., 1968. Refractive index of carbon dioxide cryodeposit. J. Appl. Phys. 39, 2968–2969.

Tizek, H., Grothe, H., Knözinger, E., 2004. Gas-phase deposition of acetonitrile: an attempt to understand Ostwald's step rule on a molecular basis. Chem. Phys. Lett. 383, 129–133.
Tomlin, S.G., 1968. Optical transmission and reflection formulae for thin films. Brit. J. Appl. Phys. (J. Phys. D) 2, 1667–1671.
Torrie, B.H., Binbrek, O.S., Strauss, M., Swainson, I.P., 2002. Phase transitions in solid methanol. J. Sol. State Chem. 166, 415–420.
Vasconcelos, F.A., Pilling, S., Rocha, W.R.M., Rothard, H., Boduch, P., Ding, J.J., 2017. Ion irradiation of pure and amorphous CH4 ice relevant for astrophysical environments. Phys. Chem. Chem. Phys. 19, 12845–12856.
Whitmer, J.C., 1974. Normal coordinate and potential energy distributions of methyl acetylene and some halogen substituted analogues. J. Molec. Struct. 21, 173–183.